Cretaceous Research 135 (2022) 105191

Contents lists available at ScienceDirect

Cretaceous Research

journal homepage: www.elsevier.com/locate/CretRes

Paleoatmospheric CO_2 oscillations through a cool middle/Late Cretaceous recorded from pedogenic carbonates in Africa

Theresa J. Orr [a,*], Christopher M. Wurster [a], Eric M. Roberts [b], Russell E. Singleton [a], Nancy J. Stevens [c,d], Patrick M. O'Connor [c,d]

[a] Earth & Environmental Sciences, James Cook University, Cairns, Australia
[b] Earth & Environmental Sciences, James Cook University, Townsville, Australia
[c] Department of Biomedical Sciences, Ohio University, Athens, OH 45701, USA
[d] Center for Ecological and Evolutionary Studies, Ohio University, Athens, OH 45701, USA

ARTICLE INFO

Article history:
Received 22 November 2021
Received in revised form
23 February 2022
Accepted in revised form 27 February 2022
Available online 4 March 2022

Keywords:
Atmospheric pCO_2
Carbon isotopes
Paleoclimate
Paleosol
Rukwa Rift

ABSTRACT

This study presents the first African pedogenic carbonate estimated atmospheric CO_2 concentrations for the Early to Late Cretaceous transition. Pedogenic carbonates have been used extensively as proxies to reconstruct past climates, yet few studies have focused on the climatic conditions of Africa during the Mesozoic. The paucity of paleoclimate data from the region represents a significant obstacle in interpreting past climate change, and thus our ability to predict future changes. Paleosol carbonate nodules were sampled from Bk horizons of seven particularly well-exposed and well-characterized paleosols through the Cretaceous Galula Formation, including four from the lower Mtuka Member (Aptian–Cenomanian) and three from the upper Namba Member (Campanian). The Cretaceous Galula Formation is a fossiliferous continental sedimentary succession of braided fluvial deposits that are well exposed in recently incised river drainages of the Rukwa Rift Basin, Tanzania. Oxygen isotope values averaged −5.6‰ and −7.2‰ VPDB for the Mtuka and Namba members, equating to mean annual temperatures of 14.5 °C and 11.2 °C, respectively. Using the stable isotope composition of pedogenic carbonates from the Mtuka Member, an average pCO_2 of 1860 ppmv was estimated for the Aptian–Cenomanian, before declining to an average of 520 ppmv in the Namba Member, during the Campanian. Atmospheric pCO_2 values fluctuated, but remained above 1000 ppmv through the middle Cretaceous, and correspond to the "cool" greenhouse period that spanned the Aptian–Albian. The gradual decline in pCO_2 (550–502 ppmv) recorded in the Namba Member paleosols occurred during Late Cretaceous cooling following the Cretaceous Thermal Maximum.

1. Introduction

Pedogenic carbonates are valuable terrestrial climate archives, with the stable isotope composition preserving atmospheric CO_2 concentration and temperature at the time of mineral precipitation. Pedogenic carbonates have been used extensively to reconstruct atmospheric pCO_2 during the Cretaceous (e.g. Nordt et al., 2002, 2003; Leier et al., 2009; Huang et al., 2012, 2013; Li et al., 2014; Li et al., 2016, 2020), using a well-established paleobarometer (Cerling, 1991). However, few studies have been conducted in the southern hemisphere, despite known latitudinal variations in atmospheric pCO_2 and its response to climate forcings (Huber et al., 2018). The southern high latitudes are considered particularly vital in examining global climate change in response to greenhouse episodes, with most data derived from marine deposits (Huber et al., 2018). More comprehensive southern hemispheric continental climate records are needed to better understand regional and global climate change in the face of greenhouse events.

Extreme warmth and elevated atmospheric CO_2 concentrations (>1000 ppmv) during the middle to Late Cretaceous have been recorded in paleosols worldwide, with evidence of decreasing pCO_2 phases through the Campanian–Maastrichtian (e.g. Ekart et al., 1999; Hong and Lee, 2012) prior to a pCO_2 spike at the K–T

* Corresponding author. College of Science and Engineering, James Cook University, 14–88 McGregor Road, Smithfield, QLD, 4878, Australia.
E-mail addresses: theresa.orr@my.jcu.edu.au (T.J. Orr), christopher.wurster@jcu.edu.au (C.M. Wurster), eric.roberts@jcu.edu.au (E.M. Roberts), russell.singleton1@my.jcu.edu.au (R.E. Singleton), stevensn@ohio.edu (N.J. Stevens), oconnorp@ohio.edu (P.M. O'Connor).

https://doi.org/10.1016/j.cretres.2022.105191
0195-6671/

boundary (e.g. Nordt et al., 2003). There is a complete lack of paleosol-derived $pCO2$ data for the Coniacian–Santonian, and only two studies for the Turonian, in which Sandler (2006) determined a range of 1450–2690 ppmv from paleosols in Israel, and Shang (2016) a range of 570–970 ppmv from strata in the southeastern Tibetan plateau. More paleosol-derived data exists for the Aptian–Cenomanian (e.g. Ekart et al., 1999; Hong and Lee, 2012; Li et al., 2014) and the Campanian–Maastrichtian (e.g. Nordt et al., 2003; Huang et al., 2013; Zhang et al., 2018a; Li et al., 2020), but with the exception of the Satpura Basin (Ghosh et al., 2005) and Narmada Valley (Andrews et al., 1995), both in India, existing data from paleosols are entirely sourced from paleo-northern hemisphere localities.

Herein we present the stable isotope composition of pedogenic carbonates from seven freshly-exposed and well-characterized paleosol profiles sampled in the Rukwa Rift Basin, southwest Tanzania. The paleosols are stratigraphically located in the Aptian–Cenomanian Mtuka and the Campanian Namba members of the Galula Formation, a unit that was situated at ~30 °S during the middle/Late Cretaceous (Scotese, 2016). In this study, the pedogenic carbonate paleobarometer of Cerling (1991) was applied to quantitatively estimate paleoatmospheric pCO_2 during the Aptian–Campanian. The results of this study provide the first paleosol-derived pCO_2 values for the middle/Late Cretaceous from the entire African continent and significantly enhance the southern hemispheric record of atmospheric CO_2 concentrations. This study also synthesises paleosol-derived atmospheric pCO_2 records for the Cretaceous and highlights potential uncertainty in pCO_2 estimations for the geologic period because of variations in the paleobarometer model parameters.

2. Background

The Rukwa Rift Basin forms part of the central segment of the Western Branch of the East African Rift System (EARS) in southwestern Tanzania (Chorowicz, 2005; Roberts et al., 2012), and covers an area of approximately 1.6×10^4 km^2 (Kilembe and Rosendahl, 1992). The center of the basin is occupied by the 165-km-long Lake Rukwa (Kjennerud et al., 2001), which at less than 16 m deep, is atypically shallow for Western Branch rift lakes (Kilembe and Rosendahl, 1992; Kjennerud et al., 2001; Roberts et al., 2004). The basin contains rift-fill sediment successions that correspond to four depositional phases that formed the Upper Paleozoic Karoo Supergroup, the Cretaceous Galula Formation, the Oligocene Nsungwe Formation and the Miocene–Recent Lake Beds strata (Roberts et al., 2012) (Fig. 1).

The Cretaceous Galula Formation is further subdivided into lower (Mtuka) and upper (Namba) members and consists entirely of non-marine deposits, including alluvial, fluvial and lacustrine mudstones, siltstones and sandstones (Fig. 1) (Roberts et al., 2010). The Mtuka Member comprises abundant conglomerates and coarse sandstones, and discontinuous mudstones and siltstones that are well exposed in the river drainages of the Galula, Tukuyu and Usevia areas (Roberts et al., 2010). The Mtuka Member has been interpreted to represent a large, braided river system flowing along the NW axis of the rift, and characterized by the presence of rare debris flow alluvial fan deposits and paleosol development within overbank and abandoned channel fill deposits (Orr et al., 2021). In contrast, the Namba Member consists of a finer grain fraction and is characterised by homogenous fine-to-medium grained sandstones, with few minor mudstone and siltstone deposits. The Namba Member is also interpreted to represent a large NW flowing fluvial system, but with no evidence of associated alluvial fan deposits and less common overbank or channel fill paleosol development. The Namba Member is exposed in the same river drainages as the Mtuka Member, with the significant addition of exposures in the Songwe area (Roberts et al., 2010).

The paleosols of the Mtuka and Namba members developed on red, subarkosic to lithic arkosic sandstones that form part of the channel fill deposits of a dynamic braidplain that likely extended from northern Malawi to eastern Democratic Republic of Congo (Roberts et al., 2010, 2012). Detailed characterization of the paleosols in order to refine sedimentological interpretations of the Galula Formation was recently conducted by Orr et al. (2021), highlighting the potential of these units for further Cretaceous climate investigation. The Mtuka paleosols are predominantly simple, single isolated profiles with abundant stage II pedogenic carbonate nodules (Orr et al., 2021). By contrast, the Namba paleosols are generally more complex, with simple, composite and compound profiles represented (Orr et al., 2021). Pedogenic carbonates in the Namba Member are less common and typically filamentous to nodular. Vertic Calcisols and calcic Argillisols are the primary paleosol types of the Mtuka and Namba members, respectively (Fig. 2).

The Galula Formation also hosts a diverse fossil assemblage of crocodyliforms, saurischian (sauropod and non-avian theropod) dinosaurs, fish and turtles (O'Connor et al., 2006; O'Connor et al., 2010; Sertich and O'Connor, 2014). These richly fossiliferous rift-fill sequences were preserved in the unique time interval during which Africa separated from South America, forming the Atlantic Ocean (Guiraud et al., 1992); although, age constraint on these sequences has been hampered by a lack of intercalated volcanics for more precise dating. However, a recent magnetostratigraphic study (Widlansky et al., 2018) consigned the Mtuka Member to the Aptian–Cenomanian and the Namba Member to the Cenomanian–Campanian, with two possible correlations proposed for the Namba Member: i) Turonian– Campanian and ii) Campanian – (lowermost) Maastrichtian. Most available data favor the latter correlation, which is more compatible with paleomagnetic poles (Widlansky et al., 2018), and consistent with nearby Campanian–Maastrichtian depositional events recorded in the Congo, Sudan, and Turkana basins (O'Connor et al., 2011; Widlansky et al., 2018). Moreover, the presence of the gondwanatherian mammal *Galulatherium jenkinsi* (O'Connor et al., 2019) from the Namba Member is also most compatible with the Campanian depositional age assignment based on the known distribution (Campanian–Paleogene) record of the clade.

3. Methods

3.1. Sample collection and analytical methods

Paleosol carbonate nodules were collected from seven Bk horizons within the Galula Formation (Aptian–Campanian) in river cuts along the Mtuka River (Figs. 1–2). Micritic samples from three different carbonate nodules (<10 mm) from each paleosol were extracted using a Dremel tool with spar phases avoided, and further crushed using a zirconia ring mill. Stable carbon and oxygen isotope compositions were determined using a Thermo Scientific GasBench III coupled to a continuous-flow Thermo Scientific DeltaV^{PLUS} isotope ratio mass spectrometer. CO_2 was evolved from carbonate by reaction with 100% orthophosphoric acid in 15 mL Exetainer vials, after atmosphere was replaced with He. Samples were equilibrated for 18 h at 25 °C prior to analysis. Repeat samples of international standards NBS-18 and NBS-19 with similar mass to unknown samples provided monitoring of accuracy, precision, and normalization of the Vienna PeeDee Belemnite (VPDB) scale. Precisions (1σ) for standards were better than 0.1 ‰ for both $\delta^{13}C$ and $\delta^{18}O$ values. The three isotopic values of different carbonate

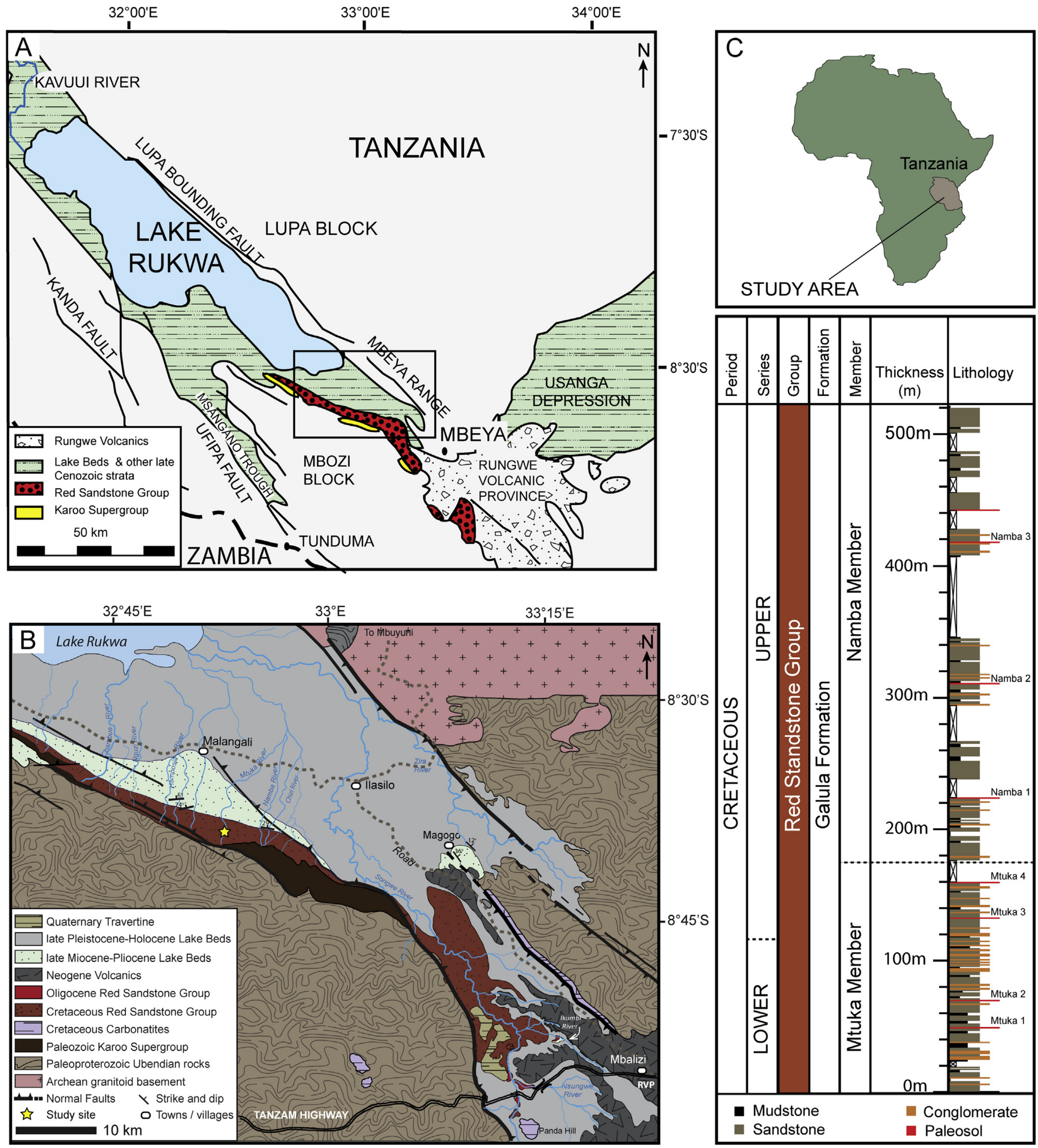

Fig. 1. A: Geologic map of the southern Rukwa Rift Basin, modified after Roberts et al. (2004). Rectangle indicates study area; B: detailed geological map of southern Rukwa Rift Basin, modified after Mtelela et al. (2017). Yellow star indicates sampling location. C: Map of Africa indicating study area in the Rukwa Rift Basin, southwest Tanzania (top). Stratotype section for the Galula Formation along the Mtuka River, modified after Roberts et al. (2004, 2010), and the stratigraphic location of the paleosols described in text (Mtuka 1–4 and Namba 1–3). (For interpretation of the references to colour in this figure legend, the reader is referred to the Web version of this article).

nodules (Fig. 3) were averaged to determine intranodule variability for each paleosol.

Bulk sediment from the uppermost horizon of each paleosol was sampled for analysis of the stable carbon isotopic composition of organic matter. After inorganic carbon was removed with 2 M HCl, samples were rinsed with Milli-Q® water, centrifuged and oven dried overnight at 60 °C. The stable carbon isotopic compositions of organic matter were determined using a Costech 4010 elemental

Fig. 2. Field photographs of the Mtuka and Namba paleosols and pedogenic carbonates. A: Mtuka 1 (vertic Calcisol); B: Mtuka 2 (vertic Argillisol); C–D: Mtuka 3 and 4 (vertic Calcisols); E: pedogenic carbonate nodules (Mtuka 3); F–G: Namba 1 and 2 (calcic Argillisols); H: Namba 3 (argillic Calcisol); I: filamentous and nodular pedogenic carbonates (Namba 1).

analyzer coupled via a ThermoScientific Conflo to a DeltaV^{Plus} isotope ratio mass spectrometer. The analytical error for organic carbon measurements is <0.2 ‰, with a mean standard deviation of 0.3 ‰ for triplicate analyses of each sample. Please refer to Table S1 for individual measurements.

All measurements were conducted at the Advanced Analytical Centre, James Cook University, Cairns. The $\delta^{13}C$ and $\delta^{18}O$ values are reported relative to VPDB, unless stated otherwise, with carbonate and organic matter samples denoted with subscripts “c” and “o”, respectively.

3.2. Atmospheric CO_2 estimation

Atmospheric CO_2 concentrations were estimated from pedogenic carbonate nodules using the paleobarometer of Cerling (1991), modified by Ekart et al. (1999).

$$pCO_2 = S(z)\left(\frac{\delta^{13}C_s - 1.0044\delta^{13}C_r - 4.4}{\delta^{13}C_a - \delta^{13}C_s}\right)$$

where pCO_2 is the concentration of CO_2 in the atmosphere (ppmv), S(z) is the concentration of CO_2 in soil (ppmv) contributed by soil respiration, and $\delta^{13}C_a$, $\delta^{13}C_r$ and $\delta^{13}C_s$ is the carbon isotopic composition of atmospheric CO_2, soil-respired CO_2, and soil CO_2, respectively. Diffusivity differences between $^{12}CO_2$ and $^{13}CO_2$ are represented by the coefficient 1.0044, with the resultant enrichment in $^{13}CO_2$ in soil CO_2 relative to soil-respired CO_2 denoted by the constant 4.4.

An average of $\delta^{13}C$ values of planktic foraminifera within Aptian–Turonian sediments, sourced from Deep Sea Drilling Project (DSDP) core 364 (Kochhann et al., 2013), International Ocean Discovery Project (IODP) site U1516 (Petrizzo et al., 2020) and Ocean Drilling Project (ODP) core 762, were selected for estimating

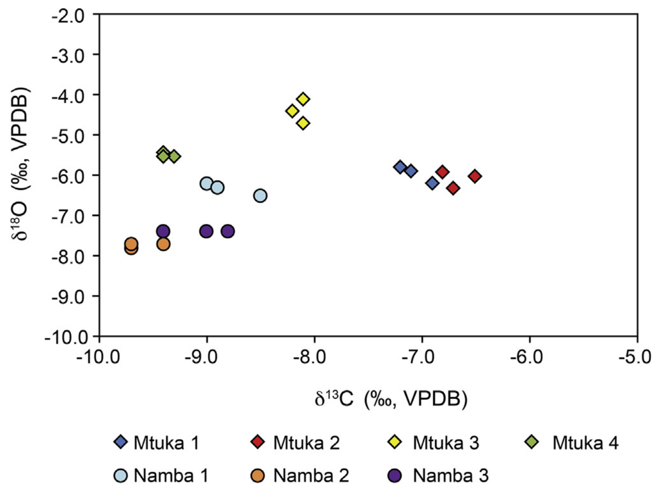

Fig. 3. Stable carbon and oxygen isotopic composition of pedogenic carbonates from the Mtuka and Namba paleosols. Measurements are the isotopic values of three different carbonate nodules sourced from each paleosol.

$\delta^{13}C_a$. An isotopic equilibrium fractionation of −7.9 ‰ between atmospheric CO_2 and planktic foraminifera was used, after Passey et al. (2002). The isotopic composition of soil-respired CO_2 ($\delta^{13}C_r$) is generally considered equal to paleosol organic carbon ($\delta^{13}C_o$) (Cerling, 1991); however, given $\delta^{13}C$ values of soil organic carbon increase with depth (Bowen and Beerling, 2004) and samples are mostly from B horizons, $\delta^{13}C_r$ was assumed to be 1‰ lower than $\delta^{13}C_o$ (Breecker and Retallack, 2014). $\delta^{13}C_s$ values were derived from pedogenic carbonate, using the temperature-dependent fractionation equation of Romanek et al. (1992), with temperatures estimated using $\delta^{18}O_c$ using the relationship found by Dworkin et al. (2005):

$$T = \frac{\delta^{18}O_c + 12.65}{0.49}$$

Although the relationship of Dworkin et al. (2005) is based on modern values, the temperature values determined by this method are considered appropriate and were not statistically different from those determined by bulk geochemistry (see Orr et al., 2021). S(z) was estimated using mean annual precipitation (MAP) values previously published (Orr et al., 2021), by the equation of Cotton and Sheldon (2012).

$$S(z) = 5.67(MAP) - 269.9$$

Standard errors for atmospheric pCO_2 estimates were calculated by Gaussian error propagation using equations derived by Retallack (2009a), which incorporates both analytical errors and transfer function-associated standard errors.

4. Results

The results of all analyses are provided in Table 1. Average temperatures ranged from 13.4 to 16.8 °C and 10.0 to 12.9 °C for the Mtuka and Namba paleosols, respectively; consistent with mean annual temperatures reported by Orr et al. (2021) for the same paleosols using bulk geochemistry and stable isotope paleothermometry. Calculations of pCO_2 from the Mtuka Member range between 1079 and 2564 ppmv for the Aptian−Cenomanian (Fig. 4), two to six times modern pCO_2 levels. Atmospheric pCO_2 oscillated through the Mtuka Member, with Mtuka 2 recording the highest concentration. Estimates of pCO_2 from the Namba Member for the Campanian are closer to modern levels and exhibit a narrow range, decreasing up-section from 555 to 502 ppmv (Fig. 4).

5. Discussion

5.1. Comparisons of pCO_2

Atmospheric pCO_2 values from the Galula Formation range between 500 and 2500 ppmv, supporting the current concept of both elevated pCO_2 values and greenhouse climate episodicity during the Cretaceous (e.g. Retallack, 2009b; Wang et al., 2014; Jing and Bainian, 2018). Our estimates for the Mtuka Member are broadly consistent with other paleosol studies of the Aptian−Cenomanian, including Ekart et al. (1999), Lee and Hisada (1999), Leier et al. (2009), Hong and Lee (2012) and Li et al. (2014), in addition to estimates based on stomatal frequencies in fossil gymnosperms (e.g. Haworth et al., 2005; Passalia, 2009). Several geochemical and isotope mass balance models are also available for comparison (e.g. GEOCARB I, II and III); for the purposes of this study, we use GEOCARBSULF (Berner, 2006). Calculated pCO_2 values for the Mtuka Member are consistent with GEOCARBSULF, although Mtuka 2 and 4 sit on the upper bounds of the error envelope (Fig. 4). Although our estimations of pCO_2 from the Namba Member are generally lower than that of other paleosol studies (e.g. Ekart et al., 1999; Nordt et al., 2002; Ghosh et al., 2005; Hong and Lee, 2012; Zhang et al., 2018a), they are consistent with estimates based on fossil stomata (e.g. Quan et al., 2009) and GEOCARBSULF. Unfortunately, the lack of magnetic reversals through the mid-Cretaceous and a lack of suitable material for radiometric dating limit the temporal resolution of our data, making more precise comparisons difficult at this time.

5.2. Variable estimations for atmospheric CO_2 *model*

The paleosol carbonate CO_2 barometer requires the estimation or assumption of several variables. In particular, the parameters S(z), $\delta^{13}C_a$ and $\delta^{13}C_r$ are frequently determined by three different approaches. S(z) is the least well constrained parameter and has been the subject of several studies (e.g. Retallack, 2009a; Breecker et al., 2010; Cotton and Sheldon, 2012). Values are typically estimated using the depth to carbonate (DTC; Retallack, 2009a) or mean annual precipitation (MAP; Cotton and Sheldon, 2012) proxies, or assigned an assumed concentration, often informed by the perceived paleoclimatic conditions (e.g. Nordt et al., 2002; Hong and Lee, 2012). Other approaches are infrequently used (e.g. soil type). $\delta^{13}C_a$ and $\delta^{13}C_r$ values are usually estimated from the $\delta^{13}C$ values of marine carbonates (MC), $\delta^{13}C$ of organic matter (OM), or assigned an assumed value. MC $\delta^{13}C$ values are typically from planktic foraminifera from marine sediments (e.g. Nordt et al., 2003; Huang et al., 2013), although benthic foraminifera have also been used (e.g. Barral et al., 2017). An isotopic equilibrium fractionation of −7.9 ‰ between atmospheric CO_2 and planktic foraminifera (Passey et al., 2002) is applied when estimating $\delta^{13}C_a$ values, with $\delta^{13}C_o$ values subsequently calculated using Arens et al. (2000) equation.

$$\delta^{13}C_a = \frac{\delta^{13}C_o + 18.67}{1.1}$$

Organic matter $\delta^{13}C$ values are occasionally sourced from occlusions in pedogenic carbonate nodules (e.g. Breecker and Retallack, 2014), but are more frequently obtained from paleosol bulk sediment (e.g. Huang et al., 2012; Li et al., 2020). The OM $\delta^{13}C$ values are either substituted directly for $\delta^{13}C_r$ (e.g. Li et al., 2020) or assume some minor fractionation (e.g. Breecker and Retallack,

Table 1
Stable isotope measurements of pedogenic carbonate and bulk sediment organic matter, and data used to estimate atmospheric CO_2 concentrations for the middle-Late Cretaceous.

Paleosol	$\delta^{13}C_c$ (‰)	$\delta^{18}O_c$ (‰)	$\delta^{13}C_a$ (‰)	$\delta^{13}C_r$ (‰)	$\delta^{13}C_s$ (‰)	S(z) (ppmv)	T (°C)	MAP (mm/yr)	pCO_2 (ppmv)	SE (ppmv)
Namba 3	−9.1	−7.4	−5.8	−25.0	−19.5	3143	10.7	602	502	59
Namba 2	−9.6	−7.7	−5.8	−25.3	−20.2	3869	10.0	730	505	41
Namba 1	−8.8	−6.3	−5.8	−24.4	−19.0	3603	12.9	683	555	55
Mtuka 4	−8.1	−4.4	−5.8	−27.5	−17.9	4606	16.8	860	2457	302
Mtuka 3	−9.4	−5.5	−5.8	−26.0	−19.4	4453	14.6	833	1079	114
Mtuka 2	−6.7	−6.1	−5.8	−27.4	−16.9	3875	13.4	731	2564	384
Mtuka 1	−7.1	−6.0	−5.8	−27.2	−17.2	2304	13.6	454	1357	337

Note 1: Values for $\delta^{13}C_c$, $\delta^{18}O_c$, $\delta^{13}C_a$, $\delta^{13}C_r$, $\delta^{13}C_s$ and T represent mean values based on three distinct nodules per paleosol unit. Refer to Table S1 for individual measurements.
Note 2: Mean annual precipitation (MAP) values are from Orr et al. (2021).

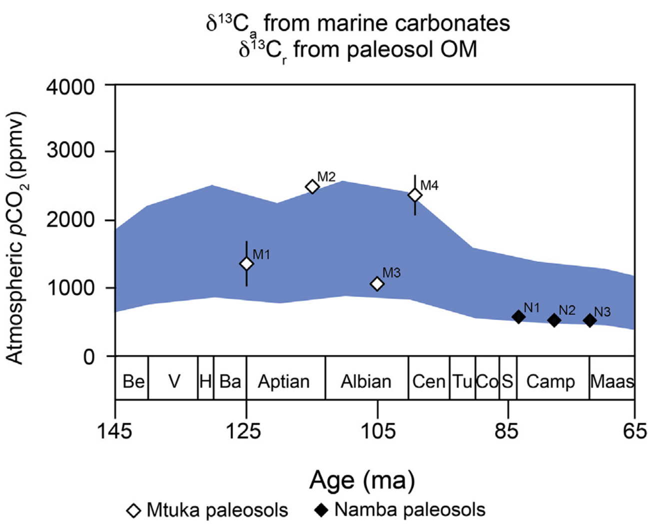

Fig. 4. Paleosol-derived atmospheric CO_2 concentrations for the Mtuka (M1–4) and Namba (N1–3) paleosols, where S(z) was estimated using the MAP proxy. $\delta^{13}C_a$ values and $\delta^{13}C_r$ values used to calculate CO_2 concentrations were derived from marine carbonates and paleosol organic matter (OM), respectively. Blue – CO_2 estimates for GEOCARBSULF (Berner, 2006). (For interpretation of the references to colour in this figure legend, the reader is referred to the Web version of this article).

2014). $\delta^{13}C_a$ values are then calculated by rearranging Arens et al. (2000) equation. When assumed, $\delta^{13}C_a$ and $\delta^{13}C_r$ values for the Cretaceous are considered to be pre-industrial values (−6.5‰), and the average isotopic composition of C_3 vegetation (−26‰), respectively (e.g. Lee, 1999).

The variations in these model assumptions lead to 27 possible iterations of the pedogenic carbonate CO_2 paleobarometer. Of these, eight iterations have been used in the literature to reconstruct atmospheric pCO_2 values during the Cretaceous. Consequently, unnecessary variation in the estimated pCO_2 values for the geologic period is likely. Given that S(z) values are the least well constrained, and have a direct proportional effect on the calculated atmospheric pCO_2 values (Cotton and Sheldon, 2012), comparisons of our estimated atmospheric pCO_2 values and the literature are evaluated first using the method of S(z) derivation.

5.2.1. DTC-derived S(z) values

The DTC proxy is a valuable means of determining a S(z) value for a given soil; however, it has limited usefulness for soil profiles that are incomplete, resulting in underestimates of S(z) (Breecker and Retallack, 2014) and consequently, potentially low atmospheric pCO_2 values. Hence, it is considered an inappropriate proxy for the Mtuka and Namba paleosols, with only two profiles retaining A horizons (Mtuka 1 and 4), albeit with erosional upper surfaces. The repeated pulses of sedimentation evident in the complex soils of the Galula Formation suggests that considerable depth/thickness may have been lost during subsequent erosional events, highlighting the inadequateness of the DTC proxy for soils in this unit. Indeed, DTC-derived S(z) values are 34–74% lower than the MAP-derived S(z) values for all paleosols, except Mtuka 1 and 4, which is expected as these are complete profiles. Application of the DTC proxy generates a broad range of pCO_2 values for the Mtuka paleosols and unreasonably low values for the Namba paleosols. Indeed, other Cretaceous paleosol studies that have used the DTC proxy for pCO_2 estimation are generally lower than the modelled values of GEOCARBSULF, although not always (Fig. 5). However, Fig. 5 also highlights the effect of varying $\delta^{13}C_a$ and $\delta^{13}C_r$ values.

Three different iterations of the pedogenic carbonate CO_2 paleobarometer using DTC-derived S(z) values were found in the literature for the Cretaceous: i) $\delta^{13}C_a$ and $\delta^{13}C_r$ paleosol OM sourced values (e.g., Li et al., 2016), ii) $\delta^{13}C_a$ and $\delta^{13}C_r$ MC sourced values (e.g., Huang et al., 2013) and iii) assumed $\delta^{13}C_a$ and $\delta^{13}C_r$ values, of −6.6 ‰ and −26 ‰ respectively (e.g., Mortazavi et al., 2013). Applying $\delta^{13}C_a$ and $\delta^{13}C_r$ paleosol OM sourced values generates the largest range of pCO_2 values (121–2792 ppmv) (Fig. 5A), and erroneously low values for most of the paleosols, with only Mtuka 1 and 4 recording values >1000 ppmv during the known greenhouse period of the Aptian–Albian. Application of $\delta^{13}C_a$ and $\delta^{13}C_r$ MC sourced values or assumed $\delta^{13}C_a$ and $\delta^{13}C_r$ values generates similarly low pCO_2 values (Fig. 5B–C), but with smaller ranges than that of the paleosol OM iteration, with values of 133–1503 ppmv and 199–1979 ppmv, respectively. Whereas the assumed $\delta^{13}C_a$ and $\delta^{13}C_r$ value iterations conforms better with GEOCARBSULF than other iterations, the estimated pCO_2 values are less useful, with the potential value gained from paleosol OM and/or marine carbonate data lost.

5.2.2. Assumed S(z) values

Assumed S(z) values provide a measure of clarity for pCO_2 reconstructions by facilitating comparisons among studies that use the same value (e.g. 5000 ppmv), but the approach has limited accuracy. The approach was first used by Cerling (1991) when developing the paleobarometer, with assumed S(z) values (~5000–10,000 ppmv) largely based on modern soil CO_2 concentrations during mean growing season. However, Breecker et al. (2009) determined that pedogenic carbonate forms in warm, dry periods and not under mean growing season conditions, as previously thought. Despite attempts to better constrain S(z) (e.g. Retallack, 2009a; Cotton and Sheldon, 2012; Breecker and Retallack, 2014) and the generation of the DTC and MAP proxies

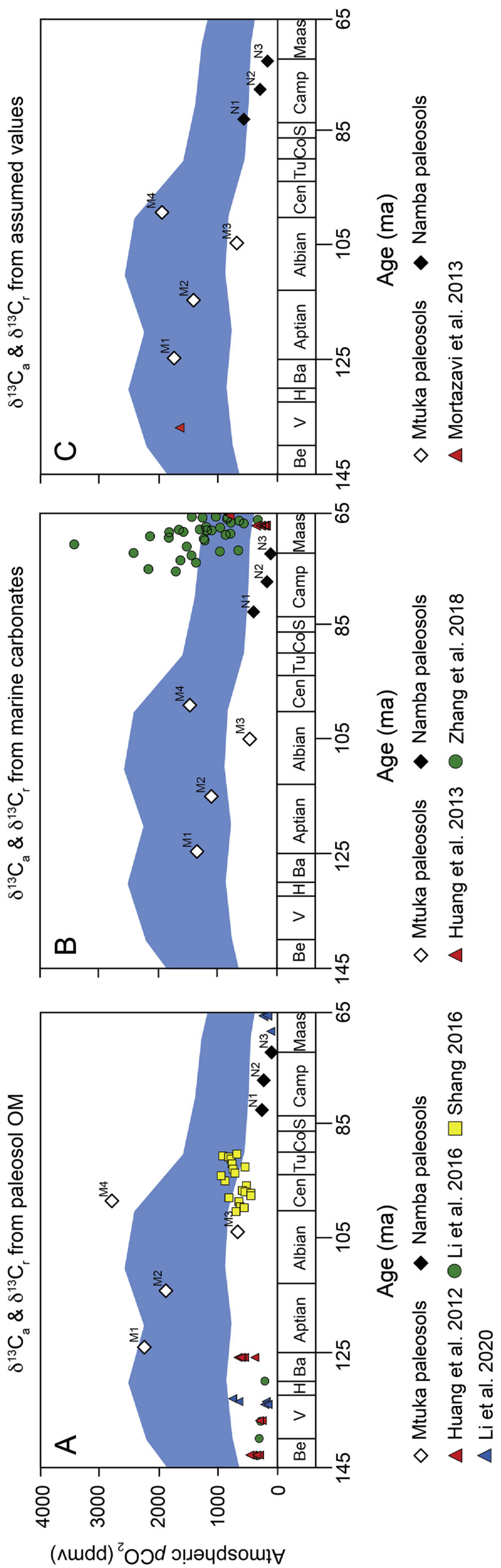

Fig. 5. Paleosol-derived atmospheric CO_2 concentrations for the Cretaceous, calculated for each iteration where S(z) was estimated using the depth to carbonate (DTC) proxy. Blue – CO_2 estimates for GEOCARBSULF (Berner, 2006); OM – organic matter. A: $\delta^{13}C_a$ and $\delta^{13}C_r$ values derived from paleosol OM; B: $\delta^{13}C_a$ and $\delta^{13}C_r$ values derived from marine carbonates; C: assumed $\delta^{13}C_a$ and $\delta^{13}C_r$ values. Data from Huang et al. (2012, 2013), Mortazavi et al. (2013), Li et al. (2016, 2020), Shang (2016), Zhang et al. (2018a) and this study (M1–4: Mtuka paleosols 1 to 4; N1–3: Namba paleosols 1 to 3). (For interpretation of the references to colour in this figure legend, the reader is referred to the Web version of this article).

from data collected during the late growing season shoulder and the warm season minimum respectively, 70% of paleosol studies that reconstructed pCO_2 for the Cretaceous used assumed and somewhat arbitrary S(z) values (Fig. 6). Of these 78% used an S(z) value of 5000 ppmv, either as an upper or lower bounding value, or as a mean value. Application of an assumed S(z) value of 5000 ppmv generates pCO_2 values that are between 9 and 117% greater than our initial calculations (Fig. 6C) and are considered overestimations.

Five different iterations of the pedogenic carbonate CO_2 paleobarometer using assumed S(z) values were found in the literature for Cretaceous sites worldwide (Fig. 6). Two iterations used $\delta^{13}C_a$ MC sourced values; one used $\delta^{13}C_r$ values sourced from MC (e.g., Robinson et al., 2002), and the other from paleosol OM (e.g., Hong and Lee, 2012). Three iterations used an assumed value for $\delta^{13}C_a$, with the $\delta^{13}C_r$ value assumed (e.g., Leier et al., 2009), or sourced from MC (e.g., Sandler, 2006) or paleosol OM (e.g., Ghosh et al., 2005).

Irrespective of the iteration, use of an assumed S(z) value generates the highest pCO_2 values for the Mtuka and Namba paleosols, with application of assumed $\delta^{13}C_a$ and $\delta^{13}C_r$ values estimating the greatest CO_2 concentrations (949–2832 ppmv) for all units, except for Mtuka 1, 2 and 4 (Fig. 6F). Application of an assumed $\delta^{13}C_a$ value and paleosol OM $\delta^{13}C_r$ values calculated the highest pCO_2 values for Mtuka 1, 2 and 4 of any iteration, recording concentrations of 3135 ppmv, 3531 ppmv and 2831 ppmv respectively (Fig. 6D). In general, application of an assumed S(z) value of 5000 ppmv generates pCO_2 values that conform to GEOCARBSULF, excluding Mtuka 1, 2 and 4, which are frequently above the error envelope (Fig. 6). Other Cretaceous paleosol studies that used assumed S(z) values are also consistent with GEOCARBSULF, but many estimates are also higher (e.g. Nordt et al., 2002, 2003; Leier et al., 2009; Hong and Lee, 2012; Li et al., 2014). Indeed, Cerling (1991) pointed out that because of the various parameter assumptions, the paleobarometer generates maximum atmospheric pCO_2 values. However, Breecker et al. (2010) determined 2500 ppmv was a more appropriate S(z) value for most paleosols and recalculated many pCO_2 values in the literature, improving the fit of the data considerably (Fig. 6A). Application of an assumed S(z) value of 2500 ppmv generates pCO_2 values for this study that are mostly below the GEOCARBSULF error envelope, nevertheless they are consistent with the recalculated pCO_2 values of Breecker et al. (2010), excluding Mtuka 1 and 2 (Fig. 6A).

5.2.3. MAP-derived S(z) values

The MAP proxy of Cotton and Sheldon (2012) allows the user to use variously sourced MAP values, such as bulk geochemistry climofunctions (e.g. CALMAG (Nordt and Driese, 2010) or the chemical index of alteration (Sheldon et al., 2002)) or morphology (e.g. DTC; Retallack, 1994, 2005) to derive an S(z) value. While the MAP proxy has been used in atmospheric pCO_2 reconstructions (e.g Cotton and Sheldon, 2012; Hyland and Sheldon, 2013), its use was not found in the Cretaceous literature. The MAP proxy was deemed the most suitable method of S(z) derivation for this study, with the DTC proxy considered inappropriate due to the truncation of the paleosols, and assumed S(z) values likely estimating less accurate pCO_2 values (excluding Mtuka 3 and 4). However, because of a lack of data, the MAP proxy should not be applied to paleosols with precipitation estimates greater than 750 mm/yr (Cotton and Sheldon, 2012). Paleoprecipitation estimates for Mtuka 3 and 4 are 833 and 860 mm/yr, respectively. Application of MAP-derived S(z) values estimate atmospheric pCO_2 values of 1079 and 2457 ppmv for Mtuka 3 and 4 respectively. Concentrations that plot within the error envelope of GEOCARBSULF and between those estimated by application of an assumed S(z) value of 2500 ppmv

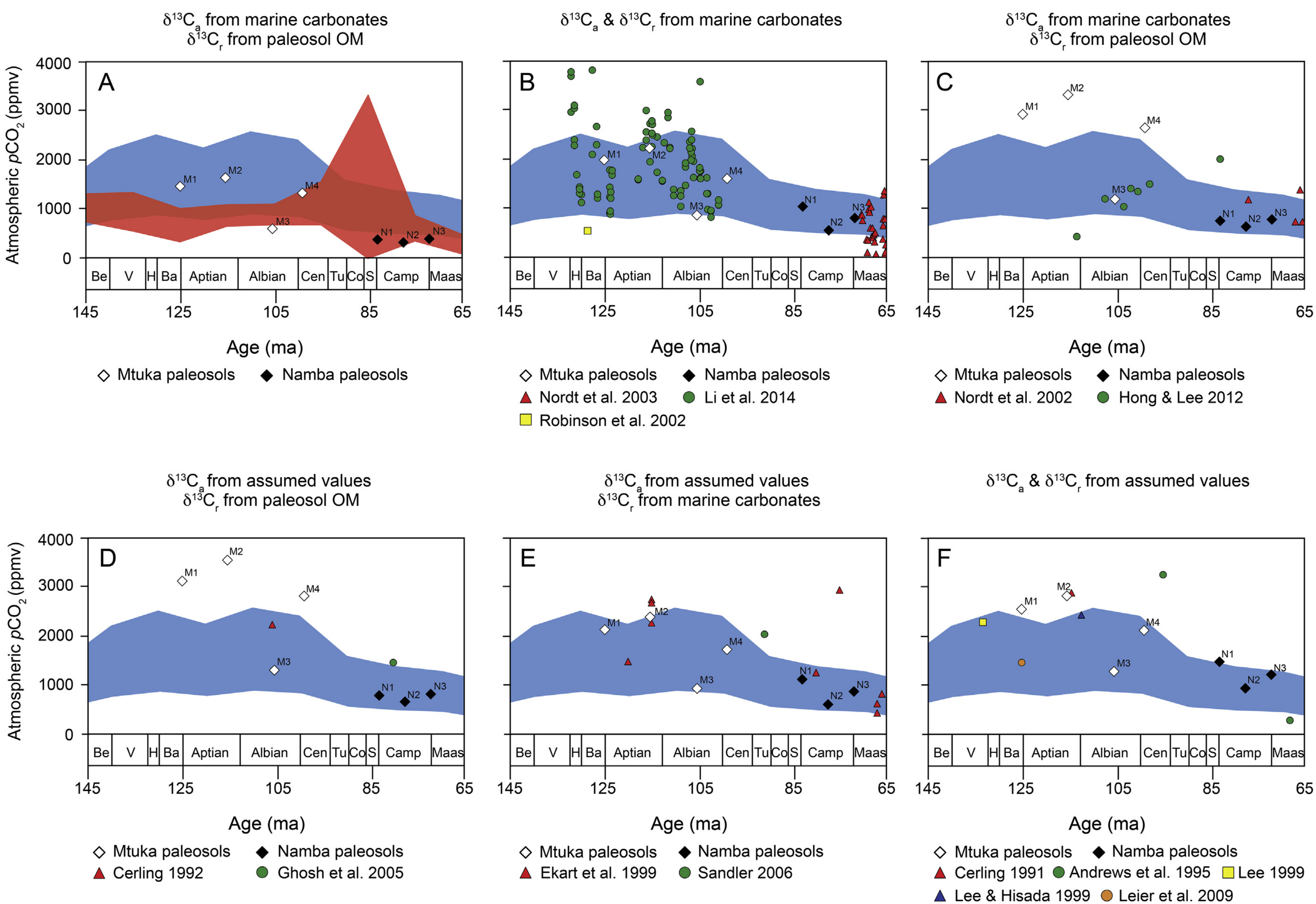

Fig. 6. Paleosol-derived atmospheric CO_2 concentrations for the Cretaceous, calculated for each iteration where S(z) was assumed. Blue shaded area – CO_2 estimates for GEOCARBSULF (Berner, 2006); OM – organic matter. A: S(z) assumed value of 2500 ppmv, $\delta^{13}C_a$ values derived from marine carbonates and $\delta^{13}C_r$ from paleosol OM for this study; Red shaded area – recalculated paleosol-derived pCO_2 values using S(z) value of 2500 ppmv from Breecker et al. (2010); B: $\delta^{13}C_a$ and $\delta^{13}C_r$ values derived from marine carbonates; C: $\delta^{13}C_a$ values derived from marine carbonates and $\delta^{13}C_r$ values from paleosol OM; D, E, F: $\delta^{13}C_a$ values are assumed, with $\delta^{13}C_r$ values from paleosol OM (D), marine carbonates (E) and assumed (F). Data from Cerling (1991, 1992), Andrews et al. (1995), Ekart et al. (1999), Lee (1999), Lee and Hisada (1999), Nordt et al. (2002, 2003), Robinson et al. (2002), Ghosh et al. (2005), Sandler (2006), Leier et al. (2009), Hong and Lee (2012), Li et al. (2014) and this study (M1–4: Mtuka paleosols 1 to 4; N1–3: Namba paleosols 1 to 3). Note – B–F: assumed S(z) value of 5000 ppmv used for data from this study. (For interpretation of the references to colour in this figure legend, the reader is referred to the Web version of this article).

(Mtuka 3: 606 ppmv; Mtuka 4: 1212 ppmv) and 5000 ppmv (Mtuka 3: 1212 ppmv; Mtuka 4: 2667 ppmv), suggesting the MAP proxy has some validity for paleosols with higher precipitation and the addition of data from soils formed in subhumid and humid areas may expand the range of this proxy.

5.3. Estimates of middle/Late Cretaceous CO_2 concentrations

Regardless of the iteration used, our paleoatmospheric pCO_2 values are consistently elevated (>1000 ppmv) during the middle Cretaceous, and decline to nearer modern levels (~500 ppmv) in the Campanian. Yet, both intervals recorded relatively cool temperatures. The high pCO_2 interval, therefore, likely corresponds to the "cool" greenhouse period of the Aptian–Albian, between Ocean Anoxic Event (OAE) 1a and OAE2, and prior to the extreme warmth of the "hot" greenhouse of the Turonian–Santonian (Huber et al., 2018). Notably, temperatures increase up section through the Mtuka Member, with a similar trend of gradual warming before the hot Greenhouse interval, as reported elsewhere (e.g. Friedrich et al., 2012). These elevated atmospheric CO_2 concentrations during the middle Cretaceous are typically attributed to enhanced volcanic outgassing (e.g. Poulsen et al., 2001). The low pCO_2 (and low temperature) interval reported here provides further evidence of gradually declining atmospheric CO_2 concentrations and temperatures during the Late Cretaceous prior to the K–T boundary (Parrish and Spicer, 1988; Andrews et al., 1995; Royer, 2006). Our data is also consistent with foraminiferal $\delta^{18}O$ values for the southern high latitudes, which similarly recorded warming in the middle Cretaceous before the hot greenhouse period of the Turonian–Santonian, and cooling through the Campanian (Huber et al., 2018).

Increased seafloor spreading rates, emplacement of large igneous provinces, super plume eruptions and volcanic arc activity have all been linked to excess greenhouse gas production during the middle Cretaceous (e.g. Hong and Lee, 2012; Huber et al., 2018). However, there is a proposed decoupling between atmospheric pCO_2 and temperature during the Aptian–Albian interval (e.g., Huber et al., 2018) with the influence of increased particulate organic carbon burial and chemical weathering of Ca and Mg silicate rocks possibly at least partially responsible for the apparent disconnect. Although, the temporal resolution of the available data also impacts our understanding of the atmospheric pCO_2 and surface temperature relationship (e.g., Wang et al., 2014). Changes in atmospheric CO_2 concentrations during the middle Cretaceous also coincide with initial radiation of angiosperms (Barrett and Willis, 2001), including the first appearance of large angiosperm trees in the late Albian (Feild et al., 2011). Angiosperm diversification accelerated in the Late Cretaceous (Lidgard and Crane, 1990), with increased vein density and leaf area thought to have given the flowering vascular plants an evolutionary advantage in the steadily declining atmospheric pCO_2 environment (Zhang et al., 2018b). Non-avian dinosaurs (e.g. hadrosaurids, ceratopsids; Lloyd et al., 2008), selected mesoeucrocodylians (e.g. notosuchians; Godoy and Turner, 2021; Stubbs et al., 2021), and mammals (e.g. Grossnickle et al., 2019) experienced similar waves of diversification in the Late Cretaceous (Lloyd et al., 2008). Whether such diversification trends among disparate terrestrial vertebrate clades represent global phenomena or regionally specific patterns awaits a better sampling (e.g. Mannion et al., 2019; Close et al., 2020), particularly from post-Cenomanian deposits from the African continent. Nevertheless, changes in atmospheric CO_2 concentrations had a wide-ranging influence on the paleoecosystems of the middle/Late Cretaceous.

6. Conclusions

In this study, the pedogenic carbonate paleobarometer was applied using MAP-derived S(z) values, $\delta^{13}C_a$ values calculated from planktic foraminifera, and $\delta^{13}C_r$ values sourced from paleosol organic matter, to estimate atmospheric pCO_2 during the Aptian–Cenomanian and Campanian. The atmospheric CO_2 concentrations are consistent with GEOCARBSULF, recording greenhouse conditions (1079–2564 ppmv) during the middle Cretaceous and lower pCO_2 conditions (550–502 ppmv) during the Late Cretaceous. These results represent the first paleosol-derived atmospheric pCO_2 values for the middle/Late Cretaceous from Africa, and only the third study of its kind for the southern hemisphere for the same interval.

Many variables contribute to a particular soil developing, consequently, S(z) values should be estimated using a proxy that takes individual soil characteristics into account (e.g. DTC or MAP). However, where erosional upper surfaces are apparent and the soil profile is incomplete (e.g. A horizon is absent) or when DTC-derived MAP values are significantly lower than bulk geochemistry-derived MAP values, the MAP proxy is considered the preferred method. If an assumed S(z) value is to be used, then 2500 ppmv is considered appropriately conservative for most soils. Marine foraminifera and paleosol organic matter are considered accurate records of $\delta^{13}C_a$ and $\delta^{13}C_r$ values, respectively.

Acknowledgements

We thank E. Maro, A. Tibaijuka, J. Temu, and F. Bassange (Tanzania Antiquties Unit, Dar es Salaam, Tanzania), M. Mashuhuri (Tanzania Commission for Science and Technology), and E. Mshui, N. Boniface, and E. Mbede (University of Dar es Salaam), and L. Kasenagala for assistance with in-country logistics and permits related to field research. We are grateful to the editor (E. Koutsoukos), M. Hendrix and two anonymous reviewers for their constructive feedback, which greatly improved the manuscript. This work was supported by the United States National Science Foundation grants [EAR-0617561, BCS-1638796 & EAR-1349825] and the James Cook University W.C. Lacy Scholarship. We would like to thank C. Mtelela and L. Lawrence for their assistance in the field, as well as the entire paleontological field crews from the Rukwa Rift Basin Project; R. Comley and J. Whan for help in the laboratory.

References

Andrews, J., Tandon, S., Dennis, P., 1995. Concentration of carbon dioxide in the Late Cretaceous atmosphere. Journal of the Geological Society 152, 1–3.
Arens, N.C., Jahren, A.H., Amundson, R., 2000. Can C3 plants faithfully record the carbon isotopic composition of atmospheric carbon dioxide? Paleobiology 26, 137–164.
Barral, A., Gomez, B., Legendre, S., Lécuyer, C., 2017. Evolution of the carbon isotope composition of atmospheric CO_2 throughout the Cretaceous. Palaeogeography, Palaeoclimatology, Palaeoecology 471, 40–47.
Barrett, P.M., Willis, K.J., 2001. Did dinosaurs invent flowers? Dinosaur—angiosperm coevolution revisited. Biological Reviews 76, 411–447.
Berner, R.A., 2006. GEOCARBSULF: a combined model for Phanerozoic atmospheric O_2 and CO_2. Geochimica et Cosmochimica Acta 70, 5653–5664.
Bowen, G.J., Beerling, D.J., 2004. An integrated model for soil organic carbon and CO_2: Implications for paleosol carbonate pCO_2 paleobarometry. Global Biogeochemical Cycles 18. GB1026.
Breecker, D., Retallack, G., 2014. Refining the pedogenic carbonate atmospheric CO_2 proxy and application to Miocene CO_2. Palaeogeography, Palaeoclimatology, Palaeoecology 406, 1–8.
Breecker, D., Sharp, Z., Mcfadden, L., 2010. Atmospheric CO_2 concentrations during ancient greenhouse climates were similar to those predicted for AD 2100. Proceedings of the National Academy of Sciences 107, 576–580.

Breecker, D., Sharp, Z., Mcfadden, L.D., 2009. Seasonal bias in the formation and stable isotopic composition of pedogenic carbonate in modern soils from central New Mexico, USA. The Geological Society of America Bulletin 121, 630–640.
Cerling, T.E., 1991. Carbon dioxide in the atmosphere: evidence from Cenozoic and Mesozoic paleosols. American Journal of Science 291, 377–400.
Cerling, T.E., 1992. Use of carbon isotopes in paleosols as an indicator of the P(CO_2) of the paleoatmosphere. Global Biogeochemical Cycles 6, 307–314.
Chorowicz, J., 2005. The East African rift system. Journal of African Earth Sciences 43, 379–410.
Close, R.A., Benson, R.B., Alroy, J., Carrano, M.T., Cleary, T.J., Dunne, E.M., Mannion, P.D., Uhen, M.D., Butler, R.J., 2020. The apparent exponential radiation of Phanerozoic land vertebrates is an artefact of spatial sampling biases. Proceedings of the Royal Society B 287, 20200372.
Cotton, J.M., Sheldon, N.D., 2012. New constraints on using paleosols to reconstruct atmospheric pCO_2. The Geological Society of America Bulletin 124, 1411–1423.
Dworkin, S., Nordt, L., Atchley, S., 2005. Determining terrestrial paleotemperatures using the oxygen isotopic composition of pedogenic carbonate. Earth and Planetary Science Letters 237, 56–68.
Ekart, D.D., Cerling, T.E., Montanez, I.P., Tabor, N.J., 1999. A 400 million year carbon isotope record of pedogenic carbonate: implications for paleoatmospheric carbon dioxide. American Journal of Science 299, 805–827.
Feild, T.S., Brodribb, T.J., Iglesias, A., Chatelet, D.S., Baresch, A., Upchurch, G.R., Gomez, B., Mohr, B.A., Coiffard, C., Kvacek, J., 2011. Fossil evidence for Cretaceous escalation in angiosperm leaf vein evolution. Proceedings of the National Academy of Sciences 108, 8363–8366.
Friedrich, O., Norris, R.D., Erbacher, J., 2012. Evolution of middle to Late Cretaceous oceans—a 55 m.y. record of Earth's temperature and carbon cycle. Geology 40, 107–110.
Ghosh, P., Bhattacharya, S., Ghosh, P., 2005. Atmospheric CO_2 during the Late Paleozoic and Mesozoic: Estimates from Indian Soils. In: Baldwin, I., et al. (Eds.), A history of atmospheric CO_2 and its effects on plants, animals, and ecosystems, vol. 177. Springer, New York. https://doi.org/10.1007/0-387-27048-5_2.
Godoy, P.L., Turner, A.H., 2021. Body size evolution in Crocodylians and their extinct relatives. eLS 1, 442–452.
Grossnickle, D.M., Smith, S.M., Wilson, G.P., 2019. Untangling the multiple ecological radiations of early mammals. Trends in Ecology & Evolution 34, 936–949.
Guiraud, R., Binks, R.M., Fairhead, J.D., Wilson, M., 1992. Chronology and geodynamic setting of Cretaceous-Cenozoic rifting in West and Central Africa. Tectonophysics 213, 227–234.
Haworth, M., Hesselbo, S.P., Mcelwain, J.C., Robinson, S.A., Brunt, J.W., 2005. Mid-Cretaceous pCO_2 based on stomata of the extinct conifer Pseudofrenelopsis (Cheirolepidiaceae). Geology 33, 749–752.
Hong, S.K., Lee, Y.I., 2012. Evaluation of atmospheric carbon dioxide concentrations during the Cretaceous. Earth and Planetary Science Letters 327, 23–28.
Huang, C., Retallack, G.J., Wang, C., 2012. Early Cretaceous atmospheric pCO_2 levels recorded from pedogenic carbonates in China. Cretaceous Research 33, 42–49.
Huang, C., Retallack, G.J., Wang, C., Huang, Q., 2013. Paleoatmospheric pCO_2 fluctuations across the Cretaceous–Tertiary boundary recorded from paleosol carbonates in NE China. Palaeogeography, Palaeoclimatology, Palaeoecology 385, 95–105.
Huber, B.T., Macleod, K.G., Watkins, D.K., Coffin, M.F., 2018. The rise and fall of the Cretaceous Hot Greenhouse climate. Global and Planetary Change 167, 1–23.
Hyland, E.G., Sheldon, N.D., 2013. Coupled CO_2-climate response during the Early Eocene Climatic Optimum. Palaeogeography, Palaeoclimatology, Palaeoecology 369, 125–135.
Jing, D., Bainian, S., 2018. Early Cretaceous atmospheric CO_2 estimates based on stomatal index of *Pseudofrenelopsis papillosa* (Cheirolepidiaceae) from southeast China. Cretaceous Research 85, 232–242.
Kilembe, E.A., Rosendahl, B., 1992. Structure and stratigraphy of the Rukwa rift. Tectonophysics 209, 143–158.
Kjennerud, T., Lippard, S., Vanhauwaert, P., 2001. Short term development of intracontinental rifts, with reference to the late Quaternary of the Rukwa Rift (East African Rift System). Marine and Petroleum Geology 18, 307–317.
Kochhann, K.G., Koutsoukos, E.A., Fauth, G., Sial, A.N., 2013. Aptian–Albian Planktic Foraminifera from DSDP Site 364 (Offshore Angola): Biostratigraphy, Paleoecology, and Paleoceanographic Significance. Journal of Foraminiferal Research 43, 443–463.
Lee, Y.I., 1999. Stable isotopic composition of calcic paleosols of the Early Cretaceous Hasandong Formation, southeastern Korea. Palaeogeography, Palaeoclimatology, Palaeoecology 150, 123–133.
Lee, Y.I., Hisada, K.I., 1999. Stable isotopic composition of pedogenic carbonates of the Early Cretaceous Shimonoseki Subgroup, western Honshu, Japan. Palaeogeography, Palaeoclimatology, Palaeoecology 153, 127–138.
Leier, A., Quade, J., Decelles, P., Kapp, P., 2009. Stable isotopic results from paleosol carbonate in South Asia: Paleoenvironmental reconstructions and selective alteration. Earth and Planetary Science Letters 279, 242–254.
Li, J., Wen, X., Huang, C., 2016. Lower Cretaceous paleosols and paleoclimate in Sichuan Basin, China. Cretaceous Research 62, 154–171.
Li, J., Wen, X., Huang, C., 2020. Lower and upper Cretaceous paleosols in the western Sichuan Basin, China: Implications for regional paleoclimate. Geological Journal 55, 390–408.
Li, X., Jenkyns, H.C., Zhang, C., Wang, Y., Liu, L., Cao, K., 2014. Carbon isotope signatures of pedogenic carbonates from SE China: rapid atmospheric pCO_2 changes during middle–late Early Cretaceous time. Geological Magazine 151, 830–849.
Lidgard, S., Crane, P.R., 1990. Angiosperm diversification and Cretaceous floristic trends: a comparison of palynofloras and leaf macrofloras. Paleobiology 16, 77–93.
Lloyd, G.T., Davis, K.E., Pisani, D., Tarver, J.E., Ruta, M., Sakamoto, M., Hone, D.W., Jennings, R., Benton, M.J., 2008. Dinosaurs and the Cretaceous terrestrial revolution. Proceedings of the Royal Society B: Biological Sciences 275, 2483–2490.
Mannion, P.D., Chiarenza, A.A., Godoy, P.L., Cheah, Y.N., 2019. Spatiotemporal sampling patterns in the 230 million year fossil record of terrestrial crocodylomorphs and their impact on diversity. Palaeontology 62, 615–637.
Mortazavi, M., Moussavi-Harami, R., Brenner, R.L., Mahboubi, A., Nadjafi, M., 2013. Stable isotope record in pedogenic carbonates in northeast Iran: Implications for Early Cretaceous (Berriasian–Barremian) paleovegetation and paleoatmospheric P(CO_2) levels. Geoderma 211, 85–97.
Mtelela, C., Roberts, E.M., Hilbert-Wolf, H.L., Downie, R., Hendrix, M.S., O'connor, P.M., Stevens, N.J., 2017. Sedimentology and paleoenvironments of a new fossiliferous late Miocene-Pliocene sedimentary succession in the Rukwa Rift Basin, Tanzania. Journal of African Earth Sciences 129, 260–281.
Nordt, L., Atchley, S., Dworkin, S.I., 2002. Paleosol barometer indicates extreme fluctuations in atmospheric CO_2 across the Cretaceous-Tertiary boundary. Geology 30, 703–706.
Nordt, L., Atchley, S., Dworkin, S.I., 2003. Terrestrial evidence for two greenhouse events in the latest Cretaceous. Geological Society of America Today 13, 4–9.
Nordt, L., Driese, S., 2010. New weathering index improves paleorainfall estimates from Vertisols. Geology 38, 407–410.
O'Connor, P.M., Krause, D.W., Stevens, N.J., Groenke, J.R., Macphee, R.D., Kalthoff, D.C., Roberts, E.M., 2019. A new mammal from the Turonian–Campanian (Upper Cretaceous) Galula Formation, southwestern Tanzania. Acta Palaeontologica Polonica 64, 65–84.
O'Connor, P.M., Sertich, J.J., Manthi, F.K., 2011. A pterodactyloid pterosaur from the Upper Cretaceous Lapurr sandstone, West Turkana, Kenya. Anais da Academia Brasileira de Ciências 83, 309–315.
O'Connor, P.M., Gottfried, M.D., Stevens, N.J., Roberts, E.M., Ngasala, S., Kapilima, S., Chami, R., 2006. A new vertebrate fauna from the Cretaceous Red Sandstone Group, Rukwa Rift Basin, southwestern Tanzania. Journal of African Earth Sciences 44, 277–288.
O'Connor, P.M., Sertich, J.J., Stevens, N.J., Roberts, E.M., Gottfried, M.D., Hieronymus, T.L., Jinnah, Z.A., Ridgely, R., Ngasala, S.E., Temba, J., 2010. The evolution of mammal-like crocodyliforms in the Cretaceous Period of Gondwana. Nature 466, 748–751.
Orr, T.J., Roberts, E.M., Wurster, C.M., Mtelela, C., Stevens, N.J., O'Connor, P.M., 2021. Paleoclimate and paleoenvironment reconstruction of paleosols spanning the Lower to Upper Cretaceous from the Rukwa Rift Basin, Tanzania. Palaeogeography, Palaeoclimatology, Palaeoecology 577, 110539.
Parrish, J.T., Spicer, R.A., 1988. Late Cretaceous terrestrial vegetation: a near-polar temperature curve. Geology 16, 22–25.
Passalia, M.G., 2009. Cretaceous pCO_2 estimation from stomatal frequency analysis of gymnosperm leaves of Patagonia, Argentina. Palaeogeography, Palaeoclimatology, Palaeoecology 273, 17–24.
Passey, B.H., Cerling, T.E., Perkins, M.E., Voorhies, M.R., Harris, J.M., Tucker, S.T., 2002. Environmental change in the Great Plains: an isotopic record from fossil horses. The Journal of Geology 110, 123–140.
Petrizzo, M.R., Huber, B.T., Falzoni, F., Macleod, K.G., 2020. Changes in biogeographic distribution patterns of southern mid-to high latitude planktonic foraminifera during the Late Cretaceous hot to cool greenhouse climate transition. Cretaceous Research 115, 104547.
Poulsen, C.J., Barron, E.J., Arthur, M.A., Peterson, W.H., 2001. Response of the mid-Cretaceous global oceanic circulation to tectonic and CO_2 forcings. Paleoceanography 16, 576–592.
Quan, C., Sun, C., Sun, Y., Sun, G., 2009. High resolution estimates of paleo-CO_2 levels through the Campanian (Late Cretaceous) based on Ginkgo cuticles. Cretaceous Research 30, 424–428.
Retallack, G.J., 1994. The environmental factor approach to the interpretation of paleosols. SSSA Special Publication 33, 31–31.
Retallack, G.J., 2005. Pedogenic carbonate proxies for amount and seasonality of precipitation in paleosols. Geology 33, 333–336.
Retallack, G.J., 2009a. Refining a pedogenic-carbonate CO_2 paleobarometer to quantify a middle Miocene greenhouse spike. Palaeogeography, Palaeoclimatology, Palaeoecology 281, 57–65.
Retallack, G.J., 2009b. Greenhouse crises of the past 300 million years. The Geological Society of America Bulletin 121, 1441–1455.
Roberts, E.M., O'connor, P.M., Gottfried, M.D., Stevens, N., Kapalima, S., Ngasala, S., 2004. Revised stratigraphy and age of the Red Sandstone Group in the Rukwa Rift Basin, Tanzania. Cretaceous Research 25, 749–759.
Roberts, E.M., O'connor, P.M., Stevens, N.J., Gottfried, M.D., Jinnah, Z.A., Ngasala, S., Choh, A.M., Armstrong, R.A., 2010. Sedimentology and depositional environments of the Red Sandstone Group, Rukwa Rift Basin, southwestern Tanzania: New insight into Cretaceous and Paleogene terrestrial ecosystems and tectonics in sub-equatorial Africa. Journal of African Earth Sciences 57, 179–212.
Roberts, E.M., Stevens, N.J., O'connor, P.M., Dirks, P., Gottfried, M.D., Clyde, W.C., Armstrong, R.A., Kemp, A., Hemming, S., 2012. Initiation of the western branch of the East African Rift coeval with the eastern branch. Nature Geoscience 5, 289.

Robinson, S.A., Andrews, J.E., Hesselbo, S.P., Radley, J.D., Dennis, P.F., Harding, I.C., Allen, P., 2002. Atmospheric pCO2 and depositional environment from stable-isotope geochemistry of calcrete nodules (Barremian, Lower Cretaceous, Wealden Beds, England). Journal of the Geological Society 159, 215–224.
Romanek, C.S., Grossman, E.L., Morse, J.W., 1992. Carbon isotopic fractionation in synthetic aragonite and calcite: effects of temperature and precipitation rate. Geochimica et Cosmochimica Acta 56, 419–430.
Royer, D.L., 2006. CO_2-forced climate thresholds during the Phanerozoic. Geochimica et Cosmochimica Acta 70, 5665–5675.
Sandler, A., 2006. Estimates of atmospheric CO_2 levels during the mid-Turonian derived from stable isotope composition of paleosol calcite from Israel. Paleoenvironmental Record and Applications of Calcretes and Palustrine Carbonates 416, 75.
Scotese, C.R., 2016. PALEOMAP PaleoAtlas for GPlates and the PaleoData Plotter Program. PALEOMAP Project. https://www.earthbyte.org/paleomap-paleoatlas-for -gplates/.
Sertich, J.J., O'Connor, P.M., 2014. A new crocodyliform from the middle Cretaceous Galula Formation, southwestern Tanzania. Journal of Vertebrate Paleontology 34, 576–596.
Shang, F., 2016. Mesozoic History of the southeastern Tibetan Plateau: Sediment Provenance, Paleoclimate, and Surface Elevation (Doctoral dissertation). West Virginia University. Retrieved from: https://researchrepository.wvu.edu/etd/6615.
Sheldon, N.D., Retallack, G.J., Tanaka, S., 2002. Geochemical climofunctions from North American soils and application to paleosols across the Eocene-Oligocene boundary in Oregon. The Journal of Geology 110, 687–696.
Stubbs, T.L., Pierce, S.E., Elsler, A., Anderson, P.S., Rayfield, E.J., Benton, M.J., 2021. Ecological opportunity and the rise and fall of crocodylomorph evolutionary innovation. Proceedings of the Royal Society B 288, 20210069.
Wang, Y.D., Huang, C.M., Sun, B.N.A., Quan, C., Wu, J.Y., Lin, Z.C., 2014. Paleo-CO_2 variation trends and the Cretaceous greenhouse climate. Earth-Science Reviews 129, 136–147.
Widlansky, S.J., Clyde, W.C., O'connor, P.M., Roberts, E.M., Stevens, N.J., 2018. Paleomagnetism of the Cretaceous Galula Formation and implications for vertebrate evolution. Journal of African Earth Sciences 139, 403–420.
Zhang, L.M., Wang, C.S., Wignall, P.B., Kluge, T., Wan, X.Q., Wang, Q., Gao, Y., 2018a. Deccan volcanism caused coupled pCO_2 and terrestrial temperature rises, and pre-impact extinctions in northern China. Geology 46, 271–274.
Zhang, M., Dai, S., Du, B., Ji, L., Hu, S., 2018b. Mid-Cretaceous hothouse climate and the expansion of early angiosperms. Acta Geologica Sinica-English Edition 92, 2004–2025.

Appendix A. Supplementary data

Supplementary data to this article can be found online at https://doi.org/10.1016/j.cretres.2022.105191.